1 Introduction

In the last decades *nanoscience* emerged as a new research field at the interface of chemistry and physics. Materials, whose properties were well-known and understood, show novel and unexpected properties when their size is reduced from bulk to just a few nanometers in one or more dimensions [1].

In general, two effects are responsible for the change in material properties upon approaching the nanoscale: First, the surface to volume ratio increases dramatically when the dimensions shrink to only a few nanometers. For example, in nanocrystals with a diameter of about $\sim 2\,\mathrm{nm}$ almost half of the atoms are located at the surface and are available for chemical reactions. At the same time, surface atoms contribute significantly to the Gibbs free energy of the nanoparticles, changing their thermodynamic properties. E.g., nanocrystals show a melting point depression as their size decreases [1].

Second, with sizes of only a few nanometer the assumption of an infinite periodicity of the crystal lattice is no longer valid. Therefore, electrons and holes feel a confinement in one, two and three dimensions, and so-called quantum wells, wires or dots are formed, respectively. Further, since the movement of charges is restricted spatially, the Coulomb interaction becomes more important.

Overall, this means that for given materials, their properties can be tuned solely by size (and morphology) variation. Perhaps one of the best-known and extensively studied examples is the size-dependence of the optical band gap in semiconductor nanocrystals [2].

1.1 Motivation

Over the last decade nanowires (NWs) became the subject of intensive research. As an advantage to zero dimensional quantum dots, one dimensional NWs can be used as building elements to arrange hierarchical superstructures for optical, optoelectronic and electrical instruments. These NWs can function as both, active devices and interconnections at the same time [3]. In addition, their internal structure serves as a guide for charge carriers and photons along one axis. Direct band gap materials are of particular interest for light emission

applications, since their radiative recombination is converted primarily into photon emission. Several pioneering studies have demonstrated the use of NWs, e.g., as gain media for lasers [4], gas sensors [5], photo sensitizers for solar cells [6], field-effect transistors [7] or as probes for biological tissues [8]. However, their diameter is typically far above the Bohr radius and thus quantization effects are less prominent. With the catalyst-based solution-liquid-solid (SLS) synthesis, NWs with diameters smaller than the Bohr radius have been prepared in larger quantities [9]. Such NWs are of special interest for devices based on their optical properties since the band gap depends on the diameter, which is relatively easy to tailor [10–14]. In fact, measurements on ensembles of NWs revealed an increase of absorption and photoluminescence (PL) peak energies with decreasing diameter [12–14].

Optical measurements on single NWs can reveal electronic band structure properties that often remain hidden in averaging experiments on ensembles. Such measurements show many interesting features, yet not all of them are fully understood. In CdSe NWs, prepared with wet-chemical methods, structural variations [10] were observed, as well as fluorescence intensity fluctuations along individual NWs [15]. Alterations in crystal structure between wurtzite and zinc blende segments, with different band gaps and offsets, were reported to lead to a formation of separated quantum mechanical systems, a model which was used to explain the "hot spots" in the PL signal [15–17], with a blinking behavior similar to quantum dots (QDs). In other experiments, however, CdSe NWs have been reported to behave like single quantum mechanical systems [18,19]. The interpretation of fluorescence data is further complicated by photobrightening effects in the presence of organic ligands [20], by agglomerates of colloidal nanoparticles [21] and by variations in ligand coverage, that may lead to spectral heterogeneity as well as different emission intensities along the wire [22].

Since micro-electronic devices like transistors in integrated circuits are approaching the nano scale limit, the traditional "top-down" approach, which relies on conventional lithography techniques, to create smaller and smaller templates, from which the device is finally built, becomes extremely expensive [23]. Therefore, the "bottom-up" approach, i.e. building devices from atoms and molecules, offers a new perspective for the miniaturization of electronic components [3]. Recent advances in wet-chemical synthesis resulted in applications of hybrid nanostructures, containing NWs in photovoltaic elements [24], photocatalysis [25] and electronic devices [26]. However, for that a detailed understanding of the relation between the morphology of the nanostructure and its electronic properties is required.

1.2 Scope of this Work

This thesis has been organized as follows: Chapter 1 provides an introduction. The second chapter gives a concise overview of the theoretical background used in this work. The crystalline structure of CdSe and CdS nanowires are described. Models, which were used to calculate the optical band gap, are explained and basic terms of electrical measurements in semiconductor devices are defined.

In the third chapter the experimental methods to synthesize nanowires are outlined and the equipment used to characterize and manipulate the nanostructures is briefly described. In particular, parameters of the components, which comprise the confocal microscope are addressed and explanations for their particular use are given.

In Chapters 4, 5 and 6 the results of this thesis are presented:

Chapter 4 describes the close connection between the diameter of a NW and their band gap. A detailed correlation between the morphology and the fluorescence of NWs was established and a model for the shift in the exciton energy was developed. Further, CdSe-carbon nanotubes hybrids were investigated by PL spectroscopy.

In Chapter 5, the interplay between the PL and photocurrent (PC) is discussed. Certain regions of CdS NWs were illuminated to locally create electron-hole pairs which in turn were separated by a bias or an external electric field.

The subject of chapter 6 are heterojunction solar cells, built from CdSe nanocrystals as absorbers and poly(3-hexylthiophene-2,5-diyl) (P3HT), a common hole-conducting polymer in organic photovoltaics. The influence of the CdSe nanoparticles on the performance of the photovoltaic cell was studied and the charge generation and diffusion processes were considered.

In Chapter 7, the results are summarized and an outlook for further experiments are given.

2 Theoretical Background

In this chapter fundamental solid state theories, underlying the interpretation of the experiments in the later chapters, are presented.

2.1 II-VI Nanowires

Nanowires (NWs) are anisotropic nanocrystals, elongated along one axis. The wires can have any length from a few 100 nm up to several 100 µm. If the diameter of the wire is small enough to induce quantization effects, they are also referred to as quantum wires or quasi-1 D structures.

Crystal Structure

At atmospheric pressure II-VI semiconductors, such as CdSe or CdS, exist in two modifications of their crystal structure: wurtzite (WZ) in a hexagonal packing and zinc blende (ZB) in a cubic packing. The two structures are sketched in figure 2.1. CdSe NWs, grown by the SLS method, typically exhibit alternating lattice modifications with average segment lengths of only a few nm along their axes [10,13]. This is illustrated in figure 2.2 a and b) by transmission electron microscopy (TEM) images. The two phases differ in their respective band structure and, in particular, electron affinities, ionization potentials and fundamental band gaps [15,16,27–29].

The hexagonal structure consists of tetrahedrally coordinated Cd^{2+} and Se^{2-} atoms, stacked in the *ABAB* pattern. Zinc blende is also built up from

	CdSe		CdS	
	WZ	ZB	WZ	ZB
a / nm	0.430	0.607	0.414	0.582
b / nm	0.430	0.607	0.414	0.582
c / nm	0.701	0.607	0.675	0.582
space group	186 $P6_3mc$	216 F43m	186 $P6_3mc$	216 F43m

Table 2.1: Lattice parameters of CdSe and CdS for wurtzite (WZ) and zinc blende (ZB) modifications.

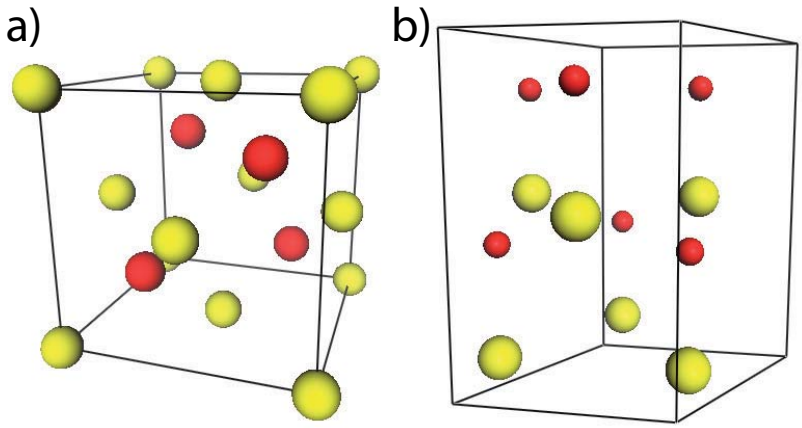

Figure 2.1: A sketch of the two possible crystal structures of CdSe: a) Zinc Blende (ZB) and b) Wurtzite (WZ) unit cell. The Cd^{2+}-ions are shown in yellow, the Se^{2-}-ions are red.

tetrahedrally coordinated atoms, but the structural pattern is *ABCABC*. The lattice parameters are given in table 2.1. Difference in inter-atomic distance between the cubic and hexagonal structure is very small along the growth axis, <1 Å, making it very difficult to distinguish between the two modifications. The differences along the a- and b-axis are around 30 % and can therefore be easily resolved. The space group is denoted with an integer from 1 to 230, followed by the Hermann-Mauguin notation. The first letter gives the Bravais lattice (*P* for primitive centering and *F* for face centred). The next three numbers and letters describe the most prominent symmetry operation visible when projected on one of the high symmetry directions of the crystal.

To determine the crystal structure of individual SLS-grown CdSe NWs they were deposited either on a copper grid with a thin carbon film or on a Si_3N_4-membrane and investigated with a transmission electron microscope (cf. section 4.1.2). In a TEM the electron beam is focused on a sample and the transmitted beam is either projected on a fluorescent screen or recorded with a digital camera. Areas with high electron density, i. e., heavy atoms, scatter electrons and appear dark in the image. In areas with low electron density, e. g., "empty space" and light atoms, the beam passes considerably unhindered and is recorded with high intensity. Therefore the TEM enables one to measure a 2-D projection of the 3-D crystal structure of the NW.

If the wire has a particular orientation, where the atomic layers are stacked behind each other, a high lattice contrast is obtained, as exemplarily shown in figure 2.2 a. Since the NWs are usually randomly oriented by the deposition, in most cases only one lattice plane can be observed, as shown in figure 2.2 b.

For a better understanding of possible orientations and the alteration between WZ and ZB segments, TEM images of a junction between these two

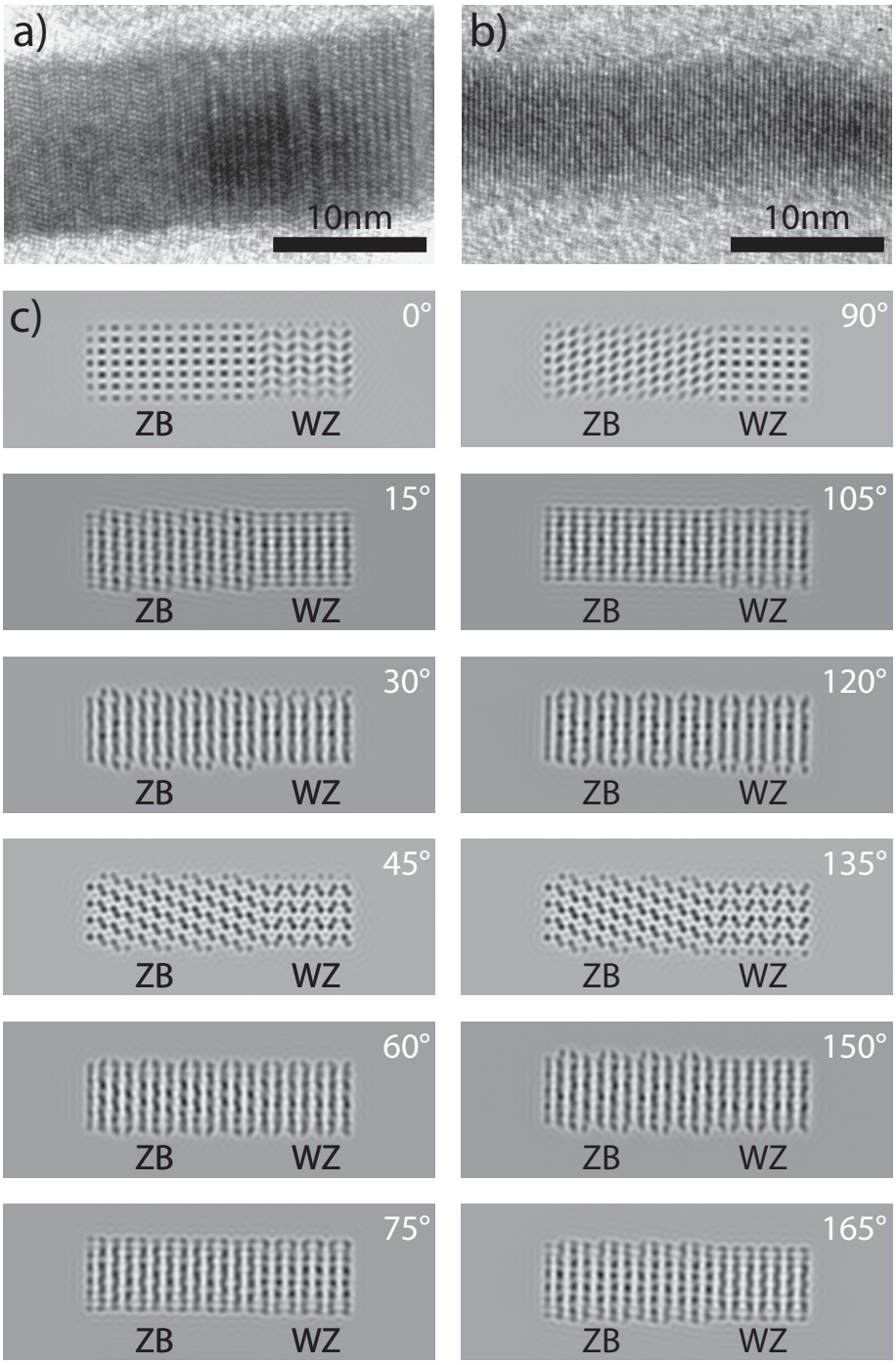

Figure 2.2: a) CdSe NW on a carbon film, the orientation corresponds to the simulated 45° image. b) A CdSe NW with an orientation, where the segments cannot be distinguished. c) Calculated TEM images, rotated in steps of 15°. The left part of the wire is zinc blende (ZB), the right segment is wurtzite (WZ). Only orientation in 45°/135° gives a clear distinction between both structures. Orientation at 0°/90° suggests that stacking faults may occur without changing between the ZB and WZ packing.

segments were simulated for different crystallographic orientations of the wire with the software SimulaTEM 1.3.2 [30]. In the simulation the specimen is cut into several slices and the propagation of an electron wave is calculated after interacting with the Coulomb potential of each of the slices. Figure 2.2 c shows the simulated TEM image of a typical wire segment in different rotations. The left part of the wire consists of ZB, the right part of WZ, merged together. The NW was rotated around its growth axis in steps of 15°. The results of the simulations show that only the orientation at 45° and 135° allows for a clear distinction between both structures. Unfortunately in real samples stacking faults may rotate the lattice during growth around its main axis, leading to a different appearance of the same phase. In addition, both phases appear the same for different orientations. In the TEM, the substrate may be rotated by up to 10°, to achieve a favorable orientation.

2.2 Effective Mass Approximation

To calculate the electronic properties of a crystalline nanostructure with many thousands of atoms, one would have to consider all interactions between every atom core and every electron. Since this is not possible with computers available today, several approximations have to be made.

The effective mass approximation transfers fundamental properties of bulk to the nano-sized material in a descriptive way. It can be derived from the nearly free electron approach, assuming the charge in a crystal behaves like a free electron with a different ("effective") mass m^*, due to the influence of the lattice.

The energy of a particle is given by

$$E = \frac{\hbar^2 k^2}{2m^*} \,, \tag{2.1}$$

with the quasi-momentum k. Without any boundary conditions, the momentum can take any value.

In the next step the influence of the lattice potential is taken into account, i.e., the Coulomb interaction of the electrons with the positively charged atom cores and other electrons in the vicinity. This leads to a phase dependence of the wave function and a discontinuity of the energy at certain k-vectors. The band diagrams of CdS and CdSe in the WZ modification are shown in figure 2.3, calculated by the pseudopotential method [31]. High symmetry points in the reciprocal space are commonly labeled with capital letters Γ, X, L, U, K and W and the electronic band structure calculations are typically performed along

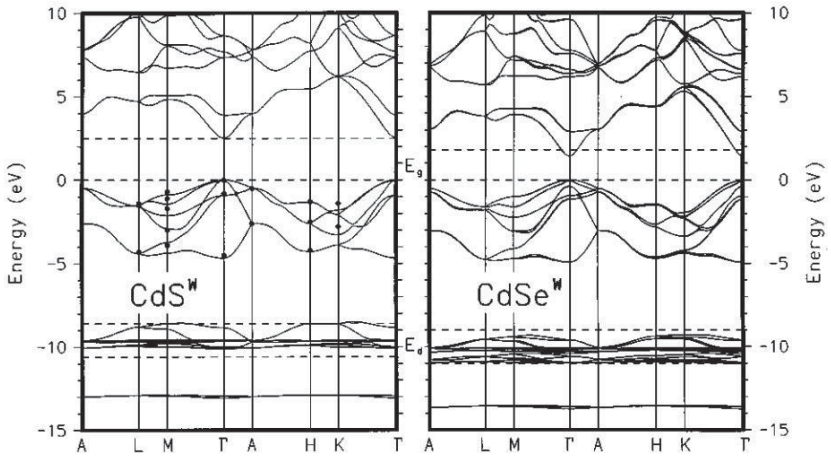

Figure 2.3: Full electronic band diagram for the WZ modification of a) CdS and b) CdSe, calculated by the pseudopotential method [31].

directions of the reciprocal space connecting such points. According to Bloch's theorem the wave functions can be separated into a plane wave and a function with the periodicity of the lattice:

$$\Psi(\mathbf{k},\mathbf{r}) = e^{i\mathbf{k}\cdot\mathbf{r}} \times \psi(\mathbf{k},\mathbf{r}) \; . \tag{2.2}$$

The effective mass of an electron in the conduction band is deduced from the energy dispersion $E(k)$ in the reciprocal space. Close to the Γ-Point, where the quasi-momentum equals zero, the conduction band is approximated by a parabola. The band curvature is referred to as the reciprocal of the effective mass:

$$\partial^2 E / \partial k^2 = \frac{\hbar^2}{m^*} \; . \tag{2.3}$$

The same consideration holds true for holes. Categorized by the valence band curvature, a distinction is made between heavy, light and split-off holes. For any given material the effective mass is a function of k and depends on the crystallographic axis.

In semiconductor-nanostructures an electron and hole can be bound by Coulomb interaction. Thus they can form a quasi-particle without a net charge, an exciton. In nanocrystals (NCs) in general and NWs in particular, the energy of an exciton can be decomposed into the fundamental band gap energy of the material E_g, the quantization energy E_q and the Coulomb interaction energy E_c:

$$E_\mathrm{exciton} = E_\mathrm{g} + E_\mathrm{q} + E_\mathrm{c} \; . \tag{2.4}$$

The Coulomb term acts over all coordinates and makes it therefore difficult to solve the Schrödinger equation. Therefore, the Coulomb interaction is disregarded when the quantization potential is calculated. Consequently, the electron and the hole do not interact with each other and the quantization energy is calculated separately for both of them. The Hamiltonian comprises then the kinetic energy of the electron and the hole in three dimensions, their confinement potential in radial direction $V_e(r,\varphi)$ and $V_h(r,\varphi)$ and the Coulomb interaction between both charges $W(\vec{r}_e - \vec{r}_h)$.

$$H = \frac{\hbar^2}{2m_e}\nabla_e^2 + V_e(r_e,\varphi_e) - \frac{\hbar^2}{2m_h}\nabla_h^2 + V_h(r_h,\varphi_h) + W(\vec{r}_e - \vec{r}_h)\ . \tag{2.5}$$

Further, the wave function is separated adiabatically into the radial coordinates r and φ on the one hand and the position of the center of mass of the exciton Z along the growth axis of the wire and the relative motion of the charges $z = z_e - z_h$ on the other hand. This is possible, because the confinement energy in radial direction, is much larger:

$$\Psi(r_e,\varphi_e,r_h,\varphi_h,Z,z) = e^{iKZ}\psi(z)\psi(r_e,\varphi_e)\psi(r_h,\varphi_h)\ . \tag{2.6}$$

The wave function, which solves the time-independent Schrödinger equation is a product of a plane wave along the wire axis and a Bessel function of the first kind in the radial direction within the wire:

$$\Psi_{m,k_z}(r,\varphi,z) = Ce^{-im\varphi}J_m\left(\frac{\beta_m}{R}r\right)e^{ik_z z}\ , \tag{2.7}$$

where C is a normalization constant and β_m is the m^{th} zero of $J_m(r)$. For the ground state of the exciton the values are $m = 0$ and $\beta_0 = 2.408$. The corresponding Hamiltonian is written as

$$H = \frac{\hbar^2}{2m_e}\nabla_e^2 + V_e(r_e,\varphi_e) - \frac{\hbar^2}{2m_h}\nabla_h^2 + V_h(r_h,\varphi_h)\ . \tag{2.8}$$

A suitable value for the depth of the potential is chosen for the environment, e.g., a ligand shell. Outside the wire, the k-vector is imaginary and the evanescent wave function is described by a MacDonald function. The continuity condition

$$\Psi(x)_{\text{in}} = \Psi(x)_{\text{out}}\ , \tag{2.9}$$